Development of a low-frost point generator operating at sub-atmospheric pressure

Development of a low-frost point generator operating at sub-atmospheric pressure

R Cuccaro[1], L Rosso, D Smorgon, G Beltramino, S Tabandeh and V Fernicola
INRiM - Istituto Nazionale di Ricerca Metrologica, Torino, I-10135, Italy

E-mail: r.cuccaro@inrim.it

Abstract

A low frost point generator (INRIM 03) operating at sub-atmospheric pressure has been designed and constructed at the Istituto Nazionale di Ricerca Metrologica (INRiM) as part of a calibration facility for upper-air sounding instruments. This new humidity generator covers the frost point temperature range between -99 °C and -20 °C and works at any controlled pressure between 200 hPa and 1100 hPa, achieving a complete saturation of the carrier gas (nitrogen) in a single passage through a stainless steel isothermal saturator. The generated humid gas contains a water vapour amount fraction between $14 \cdot 10^{-9}$ mol/mol and $5 \cdot 10^{-3}$ mol/mol. In this work the design of the generator is reported together with characterisation and performance evaluation tests. A preliminary validation of the INRIM 03 against one of the INRIM humidity standards in the common region is also included. Basing on experimental test results, an initial uncertainty evaluation of the generated frost-point temperature, T_{fp}, and water vapour amount fraction, x_w, in the limited range down to -75 °C at atmospheric pressure is reported. For the frost point temperature, the uncertainty budget yields a total expanded uncertainty (k=2) of less than 0.028 °C, while for the mole fraction the budget yields a total expanded uncertainty of less than 10^{-6} mol/mol.

Keywords: hygrometry, humidity generator, frost point, upper-air sensors

1. Introduction

The measurement of the amount of water present in material substance represent a critical aspect in several social and economics fields. Particularly, the abundance of water vapour in air and other gases influences a wide range of physical, chemical and biological processes with a significant effect on quality product, production efficiency, safety, cost, health and human comfort [1-6]. For these reasons humidity measurements play an important role in industrial, laboratory and process control applications and significant efforts to their improvement are requested by industries and beyond. Also scientists in climatology, as well as in meteorology and environmental pollution, require improvements in humidity

[1] Author to whom correspondence should be addressed

measurements, considering the fundamental role water vapour has in weather and climate change investigation. This kind of studies often require the cooperation of different groups of scientist distant in space and time and a wide use of models. To make these collaborations successful and models reliable, data of the Essential Climate Variables (EVCs) [7] need to be of high quality, consistent, unambiguous and traceable to the International System of Units (SI) [8]. Thus, also the humidity and moisture scientific community is called [9] to provide the necessary support to make this possible, as far as it is concerned.

Water vapour is one of the ECVs identified by the Global Climate Observing System (GCOS); it represents a key greenhouse gas (GHG) in the atmosphere and it is also responsible for the global water and energy cycles on Earth [10]. Despite its importance, its concentration in atmosphere and its trend over time is not yet well known. Thus, accurate measurements of ground based and airborne humidity and of its profile in atmosphere result essential to support the atmospheric and climatological research. However, since water vapour has a strong vertical concentration gradient, accurate measurements are really difficult to obtain.

Through the years, several methods and instruments have been developed for the measurement of the humidity in atmosphere [11], such as radiosondes, airborne and balloon-borne chilled mirror hygrometer (CMH), tunable diode laser absorption spectrometers (TDLAS). Among these instruments, radiosondes represent the most used measurement system to detect water vapour in the upper atmosphere. Approximately 1000 radiosondes are launched every day around the world, providing a big amount of valuable data for the determination of vertical profiles of pressure, temperature and humidity from ground to ballon-burst altitude limit, which is approximately 40 km. Once a radiosonde is assembled, its sensors of pressure, temperature and humidity are calibrated against SI traceable standards [12-14]. In particular humidity sensors are calibrated in terms of relative humidity, albeit they are much more likely dependent on water vapour partial pressure with a strong temperature sensitivity, which means there is most likely a lower bound in partial pressure detection limit, rather than in relative humidity [Vomel15]. However, this pre-launch calibration results of a little significance since strictly associated to pressure, temperature and humidity conditions at which it has been carried out [16]. In the case of radiosondes, in which operational environmental parameters vary considerably depending on the launching location and on the altitude in atmosphere, the SI-traceable calibration has to be carried out in conditions similar to those expected in the

field [17] to provide accurate and metrologically-sound humidity measurements minimizing any unwanted measurement bias or systematic error.

Considering that rising from the troposphere to the stratosphere the water vapour amount may vary between some percent to few part per million [10], in order to satisfy the demand of climatology, meteorology and aerospace community, for a standard humidity generator capable of producing a humid gas stream with a water vapour amount of the order of nmol–per–mol, during last decades some low-frost point generators have been realised in the main metrological institutes around the world. In the '90s at the National Institute of Standards and Technology (NIST) a two-temperature generator designed for the generation of precise humidity level in the frost-point range included between -100 °C and -5 °C was developed [18, 19]. This generator was a saturator based system, where the passing gas was moisturized with the evaporated and saturated water vapour rising from the ice surface. It consisted of a saturator residing within an evacuated enclosure, a flow control for carrier gas, temperature and pressure measuring instrumentation, a multimode closed loop temperature control scheme comprising Peltier heat-pump thermoelectric devices and a mechanical refrigeration system to maintain the saturator temperature stability. The expanded (k=2) relative uncertainty produced was less than 0.8% in terms of mole fraction of water vapour in air, while for humidity expressed in terms of frost-point temperature the expanded uncertainty was of 0.013 °C [20]. Based on the same phase equilibrium principle but with a complete different design, a humid gas generator in trace was developed at the D I Mendeleyev Institute for Metrology (VNIIM) [21] at the end of the last century. The system consisted of a temperature controlled chamber in which two saturators, the preliminary and the main one, were placed. Evaporated liquid nitrogen was used as a coolant in the chamber and the temperature inside the chamber was maintained equal to the required frost-point temperature. Similar to the one at NIST, in 2006 a low frost-point humidity generator was realised at the Korea Research Institute of Standards and Science (KRISS) provided with thermoelectric devices and a two-stage compression refrigerator for the temperature control. It was capable to operate from -95 °C to -40°C in the frost-point range, which corresponds to the range from 18 nmol/mol to 130 umol/mol in terms of water vapour mole fraction [22, 23]. The obtained standard uncertainty was less than 32 mK in the frost-point range from -70 °C to -40 °C, while it increased to 137 mK at -90 °C. In recent years the same generator was reformed to a two-temperature and

two-pressure type system, in order to extend the Korean institute calibration capability to a frost point of -105 °C (4 nmol/mol).The combined expanded uncertainty in the generated humidity results to be 0.72 °C (0.8 nmol/mol) when the frost point is -105 °C [24]. Generators of humidity in trace based on dilution and mixing principle were also realised, with the purpose of obtaining a faster instrument than high precision generators based upon thermodynamical equilibrium, suitable for industry applications even if a compromise in terms of accuracy is paid [25].

Although based on different principles, design and carrier gas, mentioned generators have in common the ambient pressure (~10^5 Pa) at which they work. Since radiosondes need a SI–traceable calibration in conditions similar to those encountered in atmosphere during sounding operations in terms both of pressure and water vapour mole fraction, a new low-frost point primary generator able to operate at sub-atmospheric pressure has been designed and constructed at INRIM. Indeed the generator, hereinafter called INRIM 03 in order to differentiate it from the primary humidity generators INRIM 01 and INRIM 02 already existing at the Italian national metrological institute, covers the frost-point temperature range between -99 °C and -20 °C and, in particular, works at any controlled, linearly-variable, total pressure between 1100 hPa and 200 hPa to simulate the atmospheric pressure profile from the ground level to a barometric altitude of about 12 km, where conventionally the tropopause is placed.

In this work a complete description of the generator and its performance are presented. Furthermore, a preliminary uncertainty evaluation of the generated frost-point temperature and water vapour amount fraction in the limited range down to -75 °C and at atmospheric pressure is discussed. Experimental tests include measurements of temperature gradients, pressure stability and saturator efficiency under various operating conditions, as well as a comparison between the humidity generated by the INRIM 03 and that one generated by the existing primary humidity standard INRIM 02, in the temperature and pressure overlapped region.

2. Humidity generator design and construction

INRIM 03 is a one pressure generator based on the saturation of an inert gas, specifically nitrogen, which flowing over a plan surface of isothermal ice at a well-defined temperature, *T*, and pressure, *P*, reaches the thermodynamic equilibrium with the ice. Ideally, the humid gas leaving the generator is characterised

by a water vapour mole fraction, x_w, which, for a gas saturated at a temperature T and a pressure P, is given by the following equation [26]:

$$x_w = \frac{e_w(T)}{P} \cdot f(T,P) \quad (1)$$

where $e_w(T)$ is the saturation vapour pressure in the pure phase with respect to ice at the temperature T, P is the total pressure of the gas and f is the enhancement factor, which takes into account the non-ideal behaviour of the gas. In this work the quantity $e_w(T)$ and its uncertainty are based on the Sonntag formulation [27], while the enhancement factor f is based on Greenspan's formulation for moist air [28] and its relative uncertainty $u_r(f)$ is based on the Lovell-Smith work [29] on moist air. The corresponding enhancement factor for moist N_2 was not considered as the available second virial coefficient for N_2-H_2O complex is affected by an unacceptable large uncertainty [30].

The gas humidity at the outlet of the generator can also be expressed in terms of the frost-point temperature, T_{fp}. The quantity T_{fp} is the temperature at which frost forms on cooling a gas at constant pressure and corresponds to the temperature at which gas is saturated in equilibrium with ice. Thus, in an ideal humidity generator that works perfectly, the saturation temperature T and T_{fp} correspond.

In figure 1 a schematic of the experimental apparatus and a picture of the core of the generator is presented.

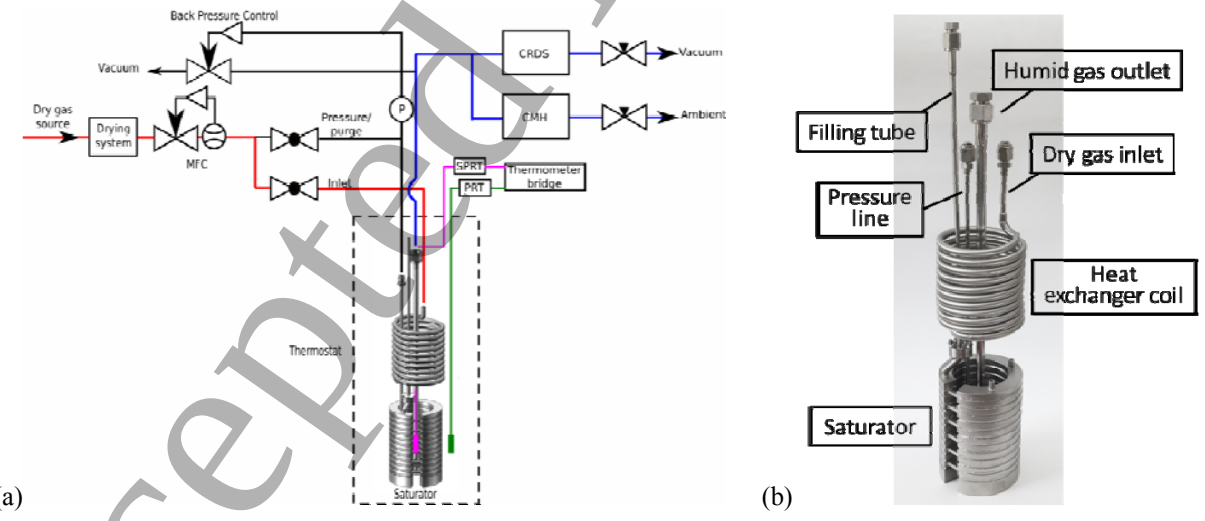

Figure 1. (a) Schematic of the experimental apparatus, which comprises the INRiM 03 low frost point generator and two humidity sensors for testing it: a CRDS (cavity ring down spectroscopy analyzer) and a CMH (chilled mirror hygrometer); (b) A picture of the core of the generator, consisting of a heat exchanger and a saturator.

A stream of dry nitrogen flows through an helicoidal heat exchanger having a length of about 3 m and then through a 3 m long stainless steel isothermal saturator. The length of the saturator has been chosen in order to ensure the complete saturation of the carrier gas with a single passage in the circuit according theory suggested by [31] and a dedicated model developed by the University of Cassino [32].

The saturator is made of stainless steel 316 L, has an height of 166 mm, an external radius of 60 mm and an internal radius of 40 mm. It is helicoidal and composed of 11 coils plus an outlet plenum, where water in excess is collected. The passageway has a cross section of 14 mm in width and 9 mm in height, of which about the 40% filled up with ice, while the remaining 60% left empty for the gas passage. The carrier gas flows from a coil to the following one passing through vertical connection holes of 8 mm of diameter. In figure 2 saturator technical details are shown.

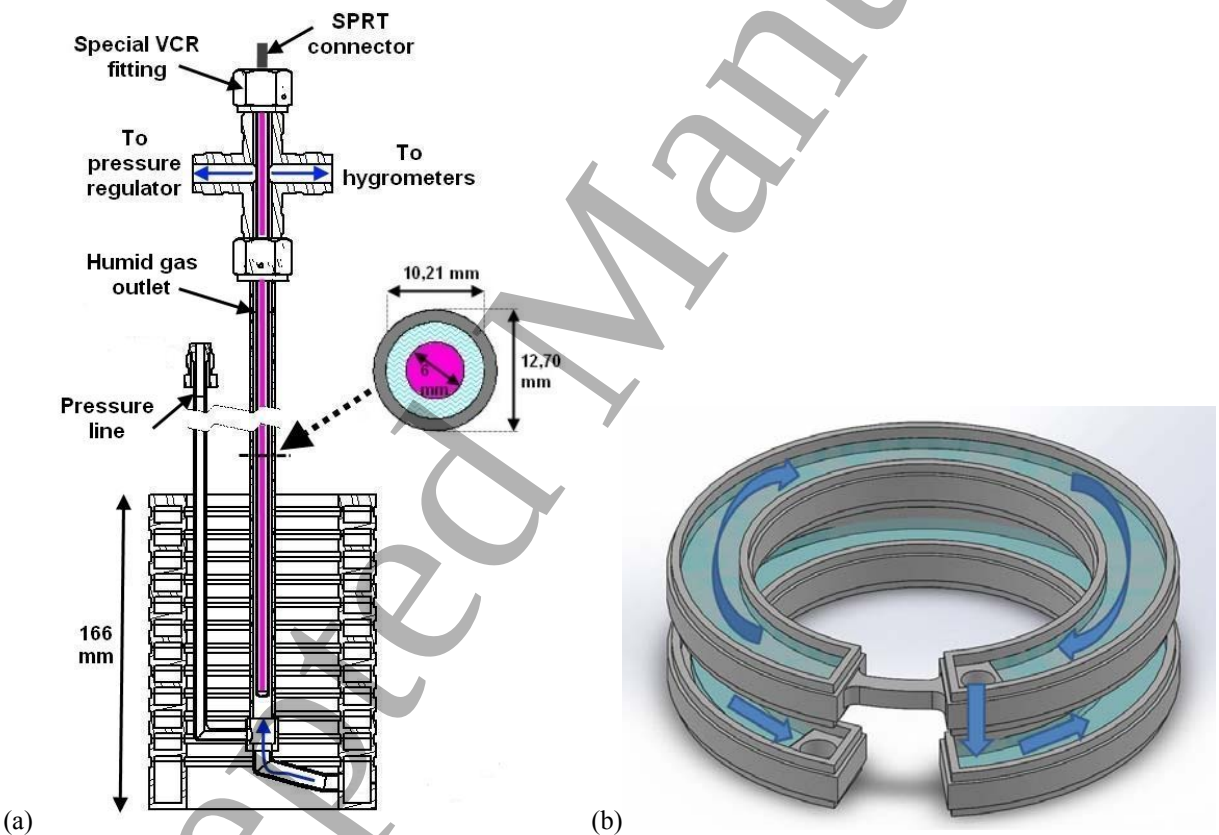

Figure 2. Engineering drawing of the saturator. a) Vertical section of the saturator with the humid gas outlet and the pressure line; the magenta line represents the SPRT, while the blue arrows show the humid gas flow direction through the outlet tube. The horizontal section of the humid gas outlet is also shown, highlighting the section reserved for the humid gas flow. b) Details about the saturator coils with the gas trajectory indicated by the arrows.

The carrier gas, saturated with water vapour, exits from the generator and passes through an electropolished tube, insulated and heated to 40 °C to avoid ice formation on its outside wall due to ambient air humidity condensation. The tube connects the generator to two different instruments placed in parallel: a cavity ring down spectroscopy analyser (CRDS) and a chilled mirror hygrometer (CMH), both used for the INRiM 03 characterisation. The CMH is used exclusively for the generator characterisation at pressure above 1000 hPa, since the sensor head is not vacuum-tight. The overpressure with respect to the ambient pressure at the inlet of the CMH is sufficient to guarantee a gas flow rate through the instrument (typically around 0.5 $l \cdot min^{-1}$). On the other hand, the CRDS works over a pressure range from 80 hPa to 2650 hPa regulating the pressure inside the cavity at 100 Torr (~ 133 hPa), so it can be used also for the INRIM 03 characterisation below 1000 hPa. However, in order to guarantee a gas flow rate (around 0.5 $l \cdot min^{-1}$) through the instrument, the outlet of the spectroscopy analyser has been connected to a vacuum pump.

The saturator and the heat exchanger are placed in a thermostatic bath, which allows to maintain a constant temperature between -99 °C and -20 °C. A standard platinum resistance thermometer (SPRT) is used to measure the saturated gas temperature, T_{sat}, which corresponds to the generated frost point temperature. It consists of a glass 25-Ω capsule SPRT assembled in a sealed 450 mm long electropolished AISI 316L sheath coaxial to the outlet pipe (see figure 2a) in thermal equilibrium with the saturated humid gas flow. The temperature of the saturator, T_{bath}, is measured by means of a secondary standard platinum resistance thermometer (PRT) immersed in the bath in such a way that the sensing element is located at the same depth of the SPRT. All temperatures are acquired by means of a precision thermometer bridge.

A back-pressure control, based on a pressure transducer to measure the saturator pressure, an electrovalve and a PID controller which sets the opening of the electrovalve toward the vacuum pump, has the function to maintain the saturator pressure at the desired constant value included between 200 hPa and 1100 hPa. The gas flow rate at the inlet of the generator, ϕ, is controlled by means of a commercial mass flow controller, with a full-scale of 10 $l \cdot min^{-1}$.

To prevent the ice formation in the heat exchanger, with a consequent block of the gas passage when the generator operate for long time at low temperature, dry inlet nitrogen must have a frost-point temperature

lower than the minimum one generated (-99 °C). For this reason, a drying system, consisting of a purifier and a molecular sieve in series, is placed before the generator inlet, in order to further reduce the frost-point temperature of the nitrogen below -100 °C. The purifier and the molecular sieve are both provided by SAES Pure Gas. The first one is a MonoTorr heated getter purifier for nitrogen gas, which withholds gaseous impurities such as oxigen and carbon dioxide present in the carrier gas by means of irreversible chemical bonds, while the second one is a MicroTorr point of use ambient temperature purifier whose removal impurities action is based on chemisorption and physisorption.

2.1. Generator filling procedure

The filling procedure of the saturator is a fundamental operation from which the correct functioning of the generator depends on. The generator is initially evacuated to about $3 \cdot 10^{-4}$ Pa to speed up the desorption from the tubing wall. Subsequently, dry nitrogen is back-fluxed through the pressure line (see figure 2a) towards the humid gas outlet bypassing the saturator coil, in order to continuously purge the outlet tubing and prevent any system contamination from the ambient. Approximately 126 ml of demineralised water are directly supplied to the first coil of the saturator through a filling tube (see figure 1b). To complete the filling procedure, dry nitrogen is now fluxed from the filling tube across the saturator to prevent ice from blocking the gas passageway, and the saturator temperature is reduced to -10 °C.

3. Performance and validation tests

In this work a preliminary uncertainty budget associated to the frost-point temperature T_{fp} and the water vapour mole fraction x_w generated by the INRiM 03 is reported. In order to determine the uncertainty sources and their impact, some performance tests have been conducted on the humidity generator, ranging in all its pressure and temperature operating range as shown in figure 3.

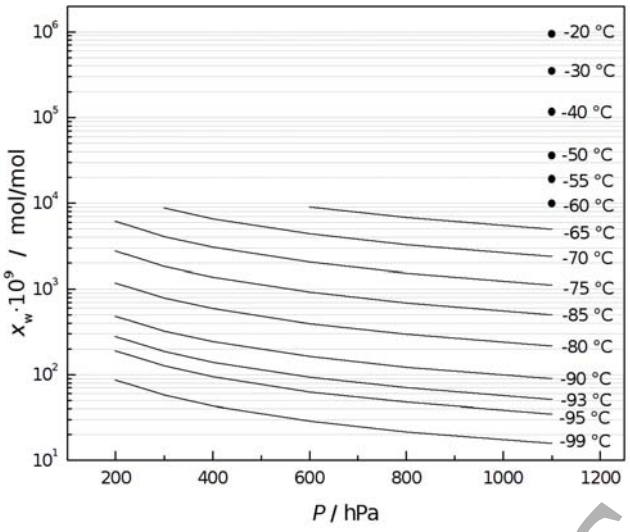

Figure 3. Characterisation of the humidity generator INRIM 03: gas pressure P, saturator temperature and corresponding water vapour mole fraction x_w range.

As shown in equation (1), x_w is influenced by variations of the pressure P, thus an evaluation of its stability is needed. After the optimization of the PID settings of the pressure controller, pressure fluctuations have been measured as a functions of the nitrogen flow rate ϕ through the generator and of the saturated gas temperature T_{sat}, in the range from 1.5 l·min^{-1} to 7 l·min^{-1} and from -20 °C to -99 °C, respectively. Measurements have been conducted in the pressure range from 200 hPa up to 1100 hPa. A pressure control stability of about 60 Pa has been routinely achieved, with a worst-case stability better than 100 Pa. Figure 4a shows the P stability as a function of time in the worst situation, corresponding to a saturator temperature of -20 °C, a flow rate of 4 l·min^{-1} and a pressure of 1100 hPa, while figure 4b shows the P stability observed at a saturator temperature of about -93 °C, flow rate 1 l·min^{-1} and a pressure of 200 hPa, which is the lowest gas pressure value investigated.

Another influence quantity is given by the gas flow rate ϕ at the inlet of the generator. Indeed, its fluctuation through the saturator implies instabilities in the gas flow rate through the chilled mirror hygrometer and, as a consequence, in the mirror temperature, increasing the uncertainty in the frost-point temperature measurements. At present the maximum peak-to-peak variation of the flow rate is about 0.006 l·min^{-1} (see figure 5a) and it has been measured at the saturator temperature of -93 °C, pressure

1100 hPa and set point flow rate of 4 l·min^{-1}. In figure 5b the flow rate variation at the saturator temperature of -99 °C, pressure 200 hPa and set point flow rate of 1.4 l·min^{-1} is shown.

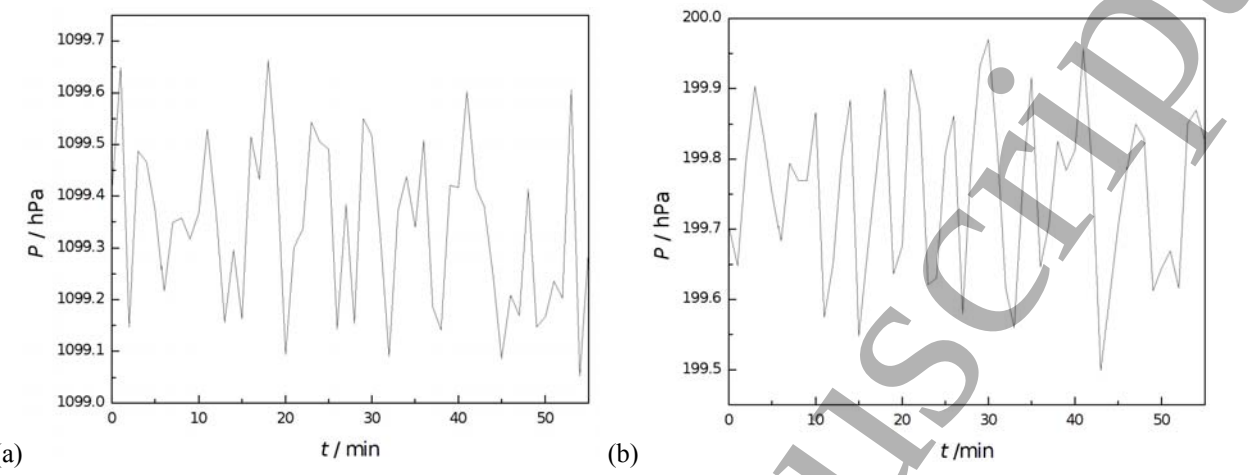

Figure 4. Pressure stability observed under the following nominal conditions: a) T_{bath} = -20 °C, ϕ = 4 l·min^{-1} and P = 1100 hPa. Peak-to-peak amplitude = 0.99 hPa, mean value = 1099.36 hPa, standard deviation = 0.18 hPa; b) T_{bath} = -93 °C, ϕ = 1 l·min^{-1} and P = 200 hPa. Peak-to-peak amplitude = 0.52 hPa, mean value = 199.76 hPa, standard deviation = 0.11 hPa.

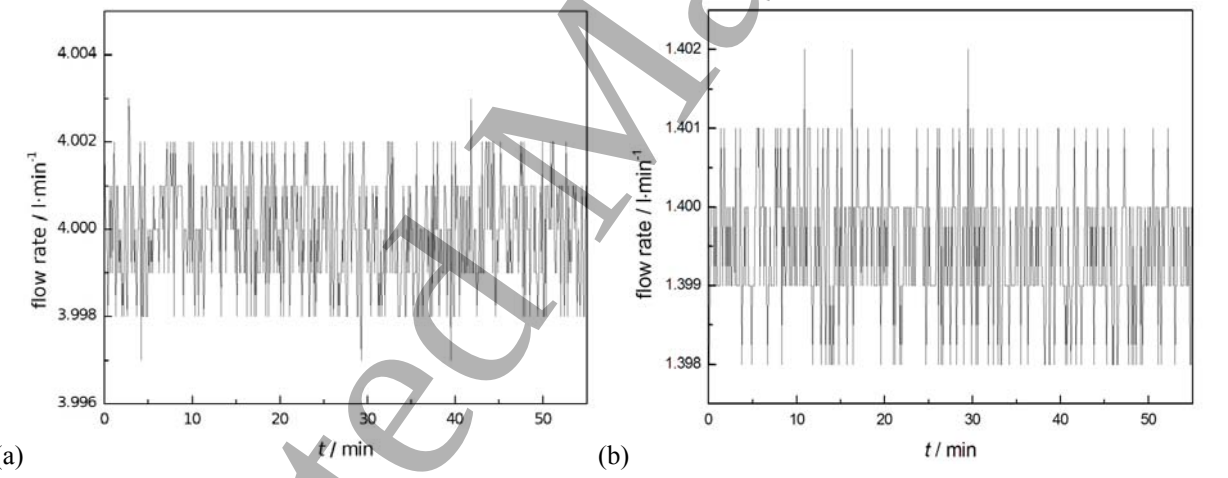

Figure 5. Flow rate stability under the following nominal conditions: a) T_{bath} = -94 °C, ϕ = 4 l·min^{-1} and P = 1100 hPa. Peak-to-peak amplitude = 0.006 l·min^{-1}, mean value = 3.999 l·min^{-1}, standard deviation = 0.001 l·min^{-1}. b) T_{bath} = -99 °C, ϕ = 1.4 l·min^{-1} and P = 200 hPa. Peak-to-peak amplitude = 0.004 l·min^{-1}, mean value = 1.400 l·min^{-1}, standard deviation = 0.001 l·min^{-1}.

The saturated gas temperature, T_{sat}, corresponds to the frost-point temperature of the humid gas generated by the INRiM 03, T_{fp}, if the water vapour of the gas is fully saturated and contributes to the determination of the water vapour amount (see equation (1)); thus an evaluation of its stability has a critical importance. Since the stability of T_{sat} depends on the stability of the temperature of the saturator, T_{bath}, the flow rate at

the inlet of the generator, ϕ, and the pressure P, its evaluation has been carried out for different values of these influence quantities. The stability of the saturated gas temperature has resulted to be better than 0.01 °C, while for the saturator temperature is better than 0.02 °C. In figure 6 and 7 an example of the T_{sat} stability is shown and compared with T_{bath}, P, and ϕ behaviour.

The generator has been designed in order to insure the water vapour saturation of the gas at the exit of the saturator. This implies that an isothermal condition through all the saturator and the outlet pipe is maintained. After have verified that T_{sat} and T_{bath} are in agreement within 0.005 °C when the thermometers are positioned at the same depth inside the bath, the saturator temperature uniformity has been evaluated moving the PRT in the bath along the height of the saturator, in particular in correspondence of the last saturator coil and repeating the measurement for different saturator temperatures. The saturator temperature uniformity is resulted better than 0.005 °C.

Finally, the saturator efficiency has been evaluated by measuring variations in x_w and T_{fp} as a function of ϕ for different values of T_{sat} and P. The carrier gas flow rate at the inlet of the generator is varied between 1.5 l·min^{-1} and 7 l·min^{-1}. In figure 8 the water vapour mole fraction and the frost-point temperature trends, measured using respectively the CRDS analyser, x_{w_CRDS}, and the CMH, T_{fp_CMH}, are reported for a saturated gas temperature and pressure of about -75 °C and 1100 hPa, while in figure 9 the quantity x_{w_CRDS} for a T_{sat} and a P of about -88 °C and 300 hPa is reported. At ambient pressure and above, the efficiency of the generator has been evaluated determining the difference between the saturated gas and the frost-point temperature measured by the chilled mirror hygrometer at different ϕ values, using as a reference the difference between T_{sat} and T_{fp_CMH} measured at 1.5 l·min^{-1}, thus assuming that at the lower flow rate the water vapour of the gas is completely saturated. Figure 10 shows the difference values determined at -75 °C and 1100 hPa. By contrast, below the ambient pressure the efficiency of the generator has been evaluated by means of the CRDS analyser comparing the theoretical water vapour mole fraction x_{w_0} determined from T_{sat} and P values with x_{w_CRDS} measured by the analyser. Figure 11shows the differences determined at a saturated gas temperature of about -75 °C and gas pressure 300 hPa.

In the evaluation of the generator efficiency, the pressure drop ΔP which occurs between the INRIM 03 outlet and the hygrometer has been also taken into account. It should be noted, the pressure drop of the gas flowing into the saturator is compensated for by design, as the system pressure is measured at a pressure tap near the last coil of the saturator.

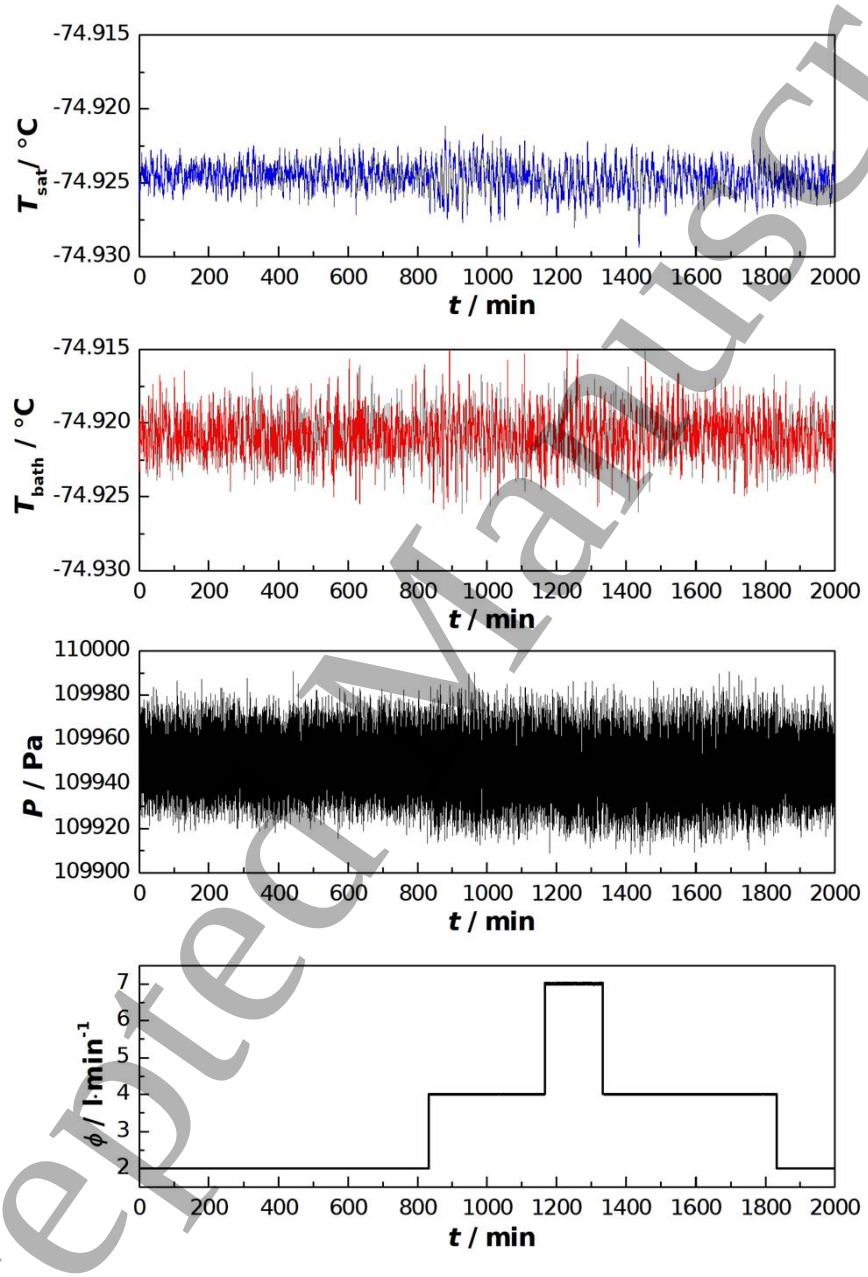

Figure 6. Saturated gas temperature T_{sat} stability at a saturator temperature T_{bath} of -75 °C, a pressure value of 1100 hPa and a flow rate included between 2 l·min^{-1} and 7 l·min^{-1}. The T_{sat} stability results to be better than 0.006 °C.

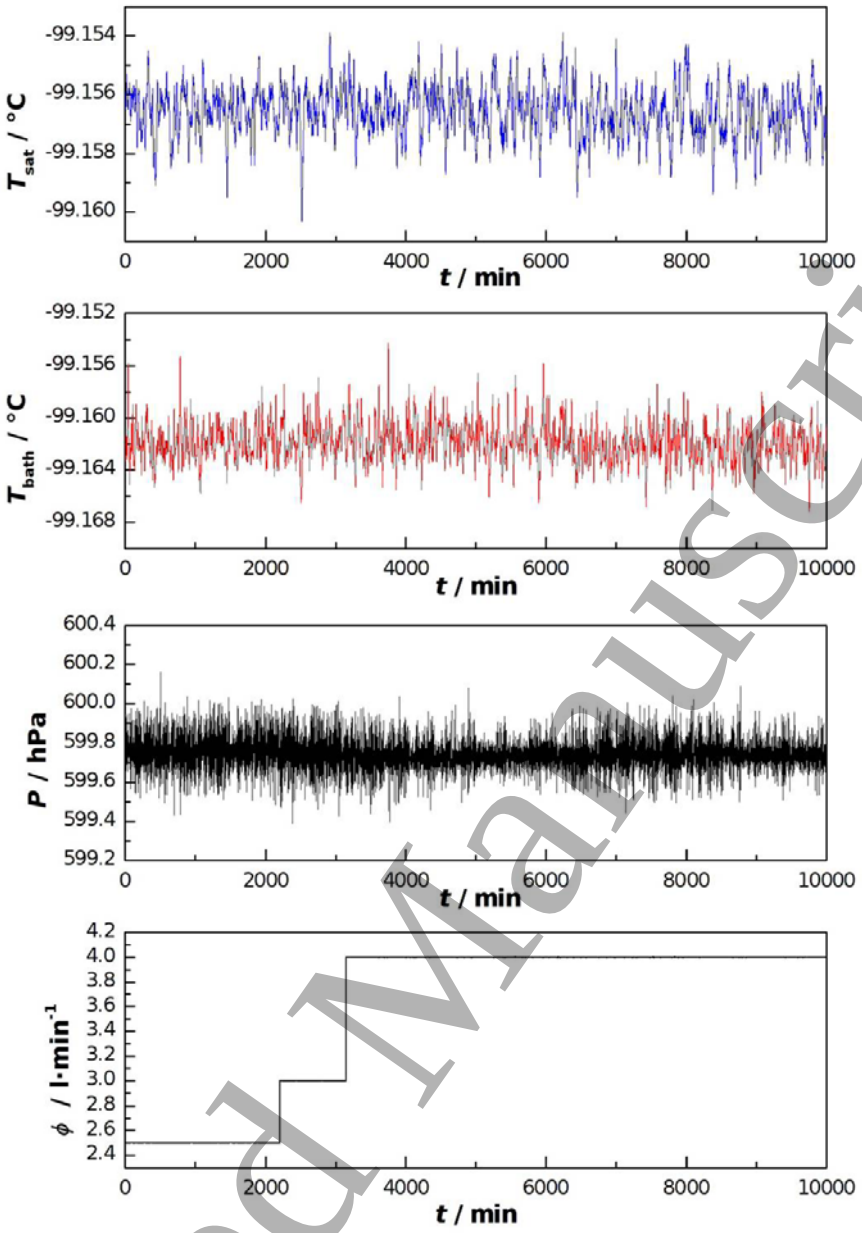

Figure 7. Saturated gas temperature T_{sat} stability at a saturator temperature T_{bath} of -99 °C, a pressure value of 600 hPa and a flow rate included between 2.5 l·min^{-1} and 4 l·min^{-1}. The T_{sat} stability results to be better than 0.007 °C.

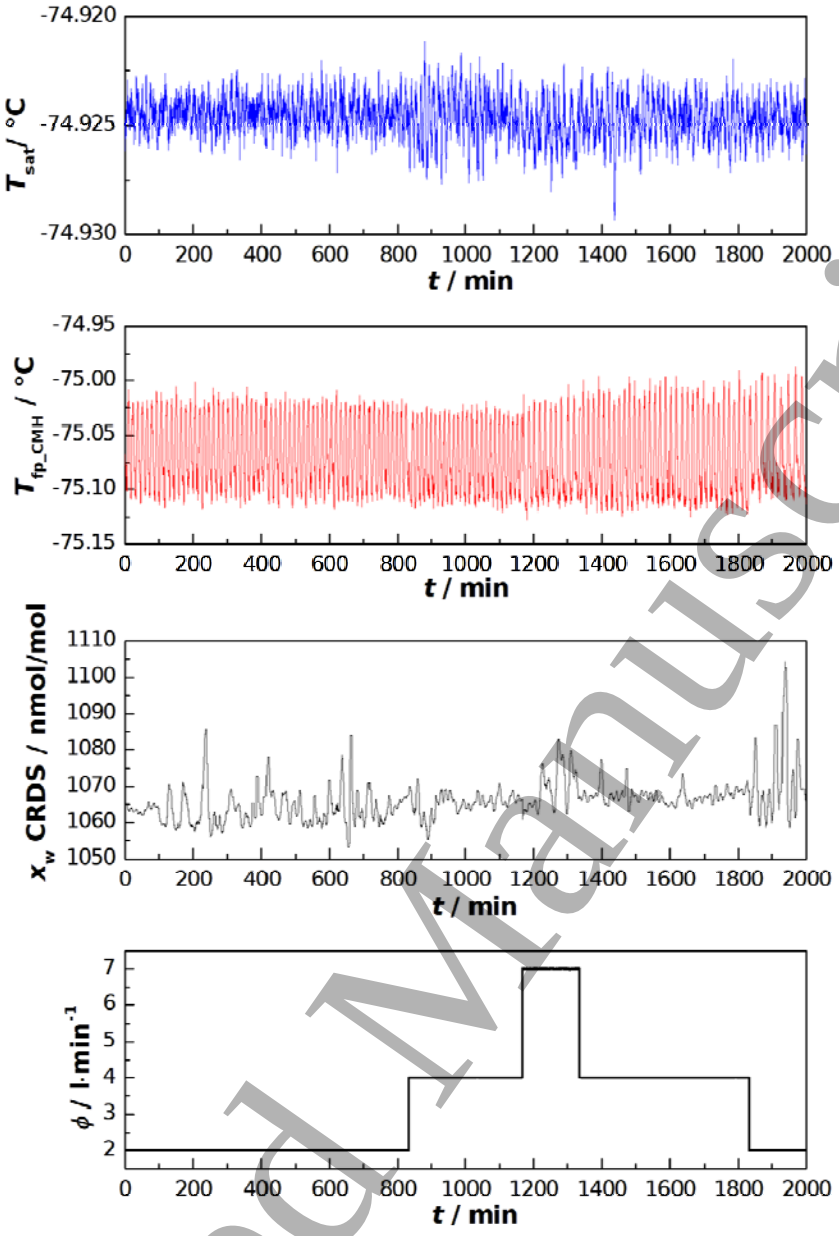

Figure 8. Trends of the water vapour mole fraction measured by the CRDS, x_{w_CRDS}, and of the frost-point temperature measured by the CMH, T_{fp_CMH}, as a function of the flow rate, ϕ, in the range between 2 l·min^{-1} and 7 l·min^{-1}. The saturated gas temperature, T_{sat}, trend is also reported in the same time range. Reported data refer to a gas pressure of about 1100 hPa.

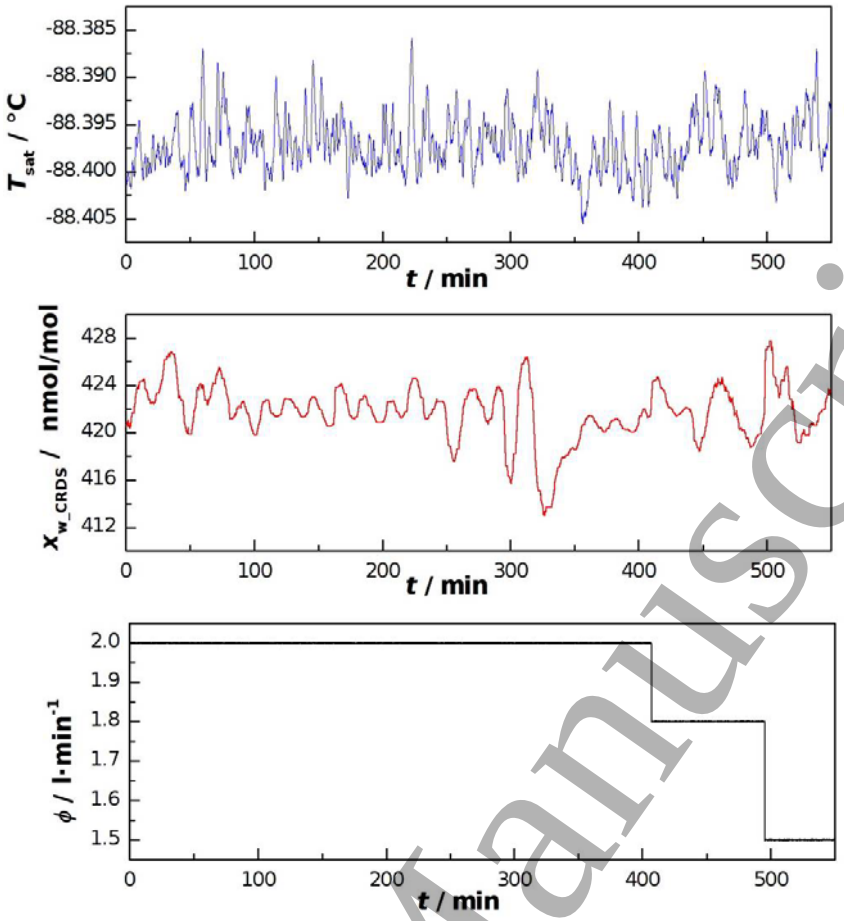

Figure 9. Trends of the water vapour mole fraction measured by the CRDS, x_{w_CRDS}, as a function of the flow rate, ϕ, in the range between 1.5 l·min^{-1} and 2 l·min^{-1}. The saturated gas temperature, T_{sat}, trend is also reported in the same time range. Reported data refer to a gas pressure of about 300 hPa.

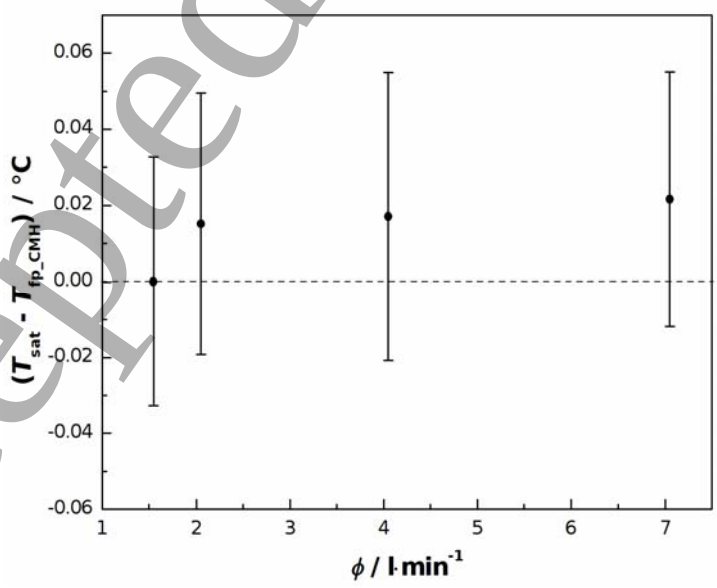

Figure 10. Differences between the saturated gas temperature, T_{sat}, and the frost-point temperature measured by the chilled mirror hygrometer, T_{fp_CMH}, as a function of the flow rate, ϕ. Reported data refer to a gas pressure of about 1100 hPa and a saturated gas temperature of about -75 °C.

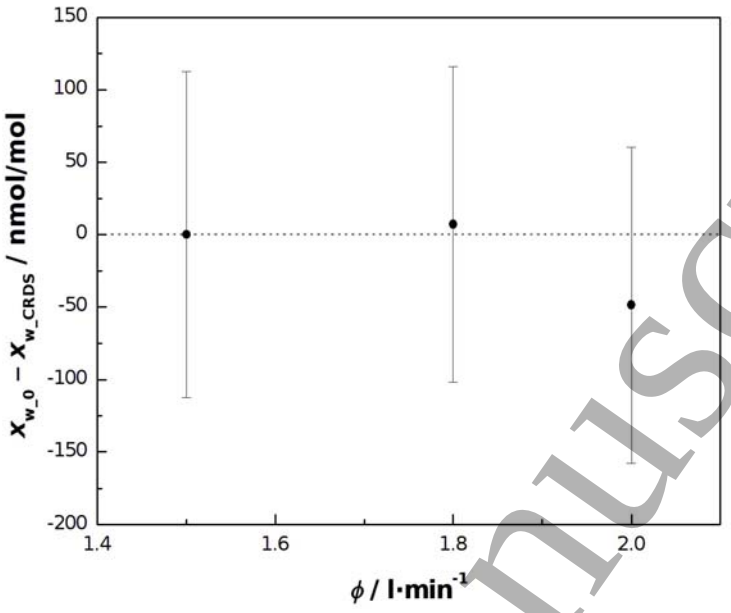

Figure 11. Differences between the theoretical water vapour mole fraction generated by the INRIM 03, x_{w_0}, and the water vapour mole fraction measured by the CRDS analyser, x_{w_CRDS}, as a function of the flow rate, ϕ. Reported data refer to a gas pressure of about 300 hPa and a saturated gas temperature of – 75 °C.

4.Uncertainty budget

Since performance tests below T_{sat} = -75 °C are still ongoing, a preliminary uncertainty budget evaluation for the mole fraction, x_w, and the frost-point temperature generated by the INRIM 03, T_{fp}, has been carried out in the temperature range between -20 °C and -75 °C at atmospheric pressure taking into account current available performance test results and specifications of the instruments which are part of the experimental apparatus. In table 1 and 2 all contributions considered to the uncertainty evaluation of T_{fp} are reported. In particular contributions relative to the specific case of the generated nominal frost-point temperature T_{fp} = -20 °C and T_{fp} = -75 °C at P = 1100 hPa are shown. By assuming that no correlation exists among quantities of influence, the combined uncertainty associated to T_{fp} is obtained as the square root of the sum of squares of each contribution weighted for its own sensitivity coefficient. In the specific case reported in table 1, the combined standard uncertainty $u_c(T_{fp})$ is 0.013 °C, while for the case reported in table 2, the combined standard uncertainty $u_c(T_{fp})$ is 0.014 °C.

Table 1. INRiM 03 uncertainty budget on the frost point temperature T_{fp} when nominally T_{fp} = -20 °C and P = 1100 hPa.

Source of uncertainty	Standard uncertainty	Probability distribution	Degrees of freedom	Sensitivity coefficient	Contribution to standard uncertainty / °C
Saturator temperature stability	0.0013 °C	Normal	>50	1	0.0013
Saturator temperature uniformity	0.0014 °C	Rectangular	>50	1	0.0014
SPRT Calibration	0.00025 °C	Normal	>50	1	0.00025
Thermometer bridge accuracy	0.00061 °C	Triangular	>50	1	0.00061
Self-heating SPRT	0.00008 Ω	Asymmetric Rectangular	>50	9.8640 °C/Ω	0.00078
Pressure drop	69 Pa	Asymmetric Rectangular	>50	0.000094 °C/Pa	0.0065
Saturation efficiency	0.0114 °C	Rectangular	>50	1	0.0114
Combined standard uncertainty, u_c					0.013

Table 2. INRiM 03 uncertainty budget on the frost point temperature T_{fp} when nominally T_{fp} = -75 °C and P = 1100 hPa.

Source of uncertainty	Standard uncertainty	Probability distribution	Degrees of freedom	Sensitivity coefficient	Contribution to standard uncertainty / °C
Saturator temperature stability	0.0008 °C	Normal	>50	1	0.0008
Saturator temperature uniformity	0.0014 °C	Rectangular	>50	1	0.0014
SPRT Calibration	0.00025 °C	Normal	>50	1	0.00025
Thermometer bridge accuracy	0.00061 °C	Triangular	>50	1	0.00061
Self-heating SPRT	0.00008 Ω	Asymmetric Rectangular	>50	9.8640 °C/Ω	0.00078
Pressure drop	69 Pa	Asymmetric Rectangular	>50	0.000058 °C/Pa	0.0040
Saturation efficiency	0.0131 °C	Rectangular	>50	1	0.0131
Combined standard uncertainty, u_c					0.014

Between the generator outlet and the inlet of the chilled mirror hygrometer used for the humidity measurement, a pressure drop up to 120 Pa was measured and taken into account in the uncertainty evaluation of T_{fp}. Considering an asymmetric rectangular probability distribution, in terms of temperature, the uncorrected pressure drop contributes to the frost-point temperature uncertainty for 0.0040 °C at T_{fp} = -75 °C and 0.0065 °C at T_{fp} = -20 °C.

As table 1 and 2 highlight, the saturation efficiency represents the main source of uncertainty to the overall T_{fp} uncertainty budget. Its contribution has been determined considering a rectangular probability distribution of the difference between T_{sat} and T_{fp_CMH} for P values above ambient pressure and between x_{w_0} and x_{w_CRDS} for P below 1000 hPa, as described in section 3.

In figure 12 contributions to the frost-point temperature uncertainty considered in the present work are depicted. The combined standard uncertainty $u_c(T_{fp})$ is also represented.

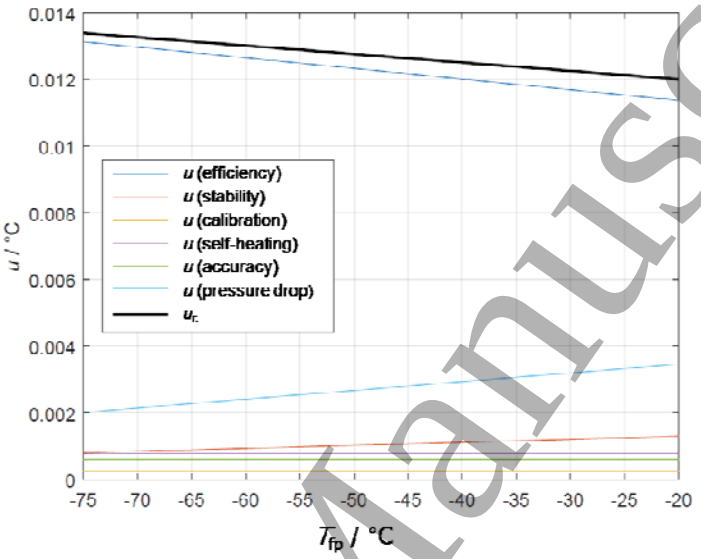

Figure 12. Sources of uncertainty and their contributions to the frost-point temperature uncertainty $u(T_{fp})$ in the temperature range -75°C to -20 °C . The thickest black line represents the combined standard uncertainty $u_c(T_{fp})$.

Starting from equation (1) and applying the uncertainty propagation law, the uncertainty associated to the water vapour mole fraction has be obtained [33]. In table 3 and 4 are reported the sources of uncertainty and their contributions for a particular case, respectively nominal T_{fp} = -20 °C, P =1100 hPa, which corresponds to a water vapour amount of $944 \cdot 10^{-6}$ mol/mol and nominal T_{fp} = -75 °C, P =1100 hPa, which corresponds to a water vapour amount of $1 \cdot 10^{-6}$ mol/mol.

Table 3. INRiM 03 water vapour mole fraction uncertainty budget when nominally $x_w = 944 \cdot 10^{-6}$ mol/mol (T_{fp} = -20 °C and P = 1100 hPa).

Source of uncertainty	Standard uncertainty	Probability distribution	Degrees of freedom	Sensitivity coefficient	Contribution to standard uncertainty mol/mol
Pure water vapour saturation pressure, $e(T_{fp})$	0.112 Pa	Normal	>50	$9 \cdot 10^{-6}$	$1 \cdot 10^{-6}$
Enhancement factor, $f(T_{fp}, P)$	0.0002 mol/mol	Normal	>50	$9 \cdot 10^{-4}$	$2 \cdot 10^{-7}$

Frost point temperature, T_{fp}	0.015 °C	Normal	>50	$7 \cdot 10^{-7}$	$8 \cdot 10^{-9}$
Saturator pressure, P	28 Pa	Normal	>50	$8 \cdot 10^{-9}$	$2 \cdot 10^{-7}$
Combined standard uncertainty, u_c					$1 \cdot 10^{-6}$

Table 4. INRiM 03 water vapour mole fraction uncertainty budget when nominally $x_w = 1 \cdot 10^{-6}$ mol/mol (T_{fp} = -75 °C and P = 1100 hPa).

Source of uncertainty	Standard uncertainty	Probability distribution	Degrees of freedom	Sensitivity coefficient	Contribution to standard uncertainty mol/mol
Pure water vapour saturation pressure, $e(T_{fp})$	0.0005 Pa	Normal	>50	$9 \cdot 10^{-6}$	$4.6 \cdot 10^{-9}$
Enhancement factor, $f(T_{fp}, P)$	0.0003 mol/mol	Normal	>50	$9 \cdot 10^{-7}$	$2.7 \cdot 10^{-10}$
Frost point temperature, T_{fp}	0.016 °C	Normal	>50	$7 \cdot 10^{-7}$	$9.7 \cdot 10^{-9}$
Saturator pressure, P	28 Pa	Normal	>50	$8 \cdot 10^{-12}$	$2.4 \cdot 10^{-10}$
Combined standard uncertainty, u_c					$1.1 \cdot 10^{-8}$

In figure 13 the uncertainty contributions to the water vapour mole fraction $u_r(x_w)$ together with the combined uncertainty $u_{cr}(x_w)$ are shown as relative contributions for all the x_w range investigated. It is worth noticing that for low values of x_w the main contribution to its uncertainty is given by T_{fp}, while for higher values it is represented by the formulation of pure water vapour saturation pressure $e(T_{fp})$.

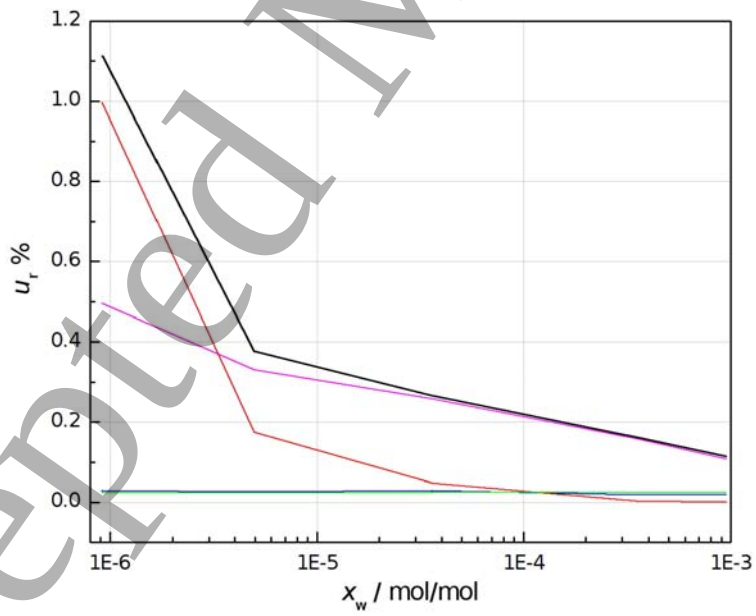

Figure 13. Sources of uncertainty and their contribution to the water vapour mole fraction relative uncertainty $u_r(x_w)$ in the mole fraction range between 10^{-6} mol/mol and 10^{-3} mol/mol. The thickest black line represents the combined relative standard uncertainty $u_{cr}(x_w)$, while the red, magenta, blue and green lines represent the relative standard uncertainties $u_r(T_{fp})$, $u_r(e(T_{fp}))$, $u_r(f(T_{fp},P))$ and $u_r(P)$ respectively.

5. Initial experimental validation

To validate the performance of the new low frost-point generator, a comparison with the standard humidity generator INRiM 02 [34-37], which works at atmospheric pressure and over the frost-point temperature range from -75 °C to 0 °C, has been performed. The comparison, by using an uncalibrated chilled mirror hygrometer (MBW 373 LX) as transfer standard, has been carried out at two different saturated gas temperatures, i.e. -20 °C and -75 °C, which belong to the working range of both generators, at P = 1100 hPa and ϕ = 1.5 l·min^{-1}. The differences between the frost-point temperature generated by the INRIM 03, $T_{\mathrm{fp\_03}}$, and the frost-point temperature generated by the INRIM 02, $T_{\mathrm{fp\_02}}$, determined as:

$$T_{\mathrm{fp\_03}} - T_{\mathrm{fp\_02}} = \left(T_{\mathrm{fp\_03}} - T_{\mathrm{fp\_CMH}}\right) - \left(T_{\mathrm{fp\_02}} - T_{\mathrm{fp\_CMH}}\right), \tag{2}$$

are shown in figure 14. The combined standard uncertainties $u_{\mathrm{c}}(T_{\mathrm{fp\_03}} - T_{\mathrm{fp\_02}})$ have been determined according to the following expression:

$$u_{\mathrm{c}}\left(T_{\mathrm{fp\_03}} - T_{\mathrm{fp\_02}}\right) = \sqrt{u^2_{T_{\mathrm{fp\_03}} - T_{\mathrm{fp\_CMH}}} + u^2_{T_{\mathrm{fp\_02}} - T_{\mathrm{fp\_CMH}}} + 2 \cdot \rho \cdot u_{T_{\mathrm{fp\_03}} - T_{\mathrm{fp\_CMH}}} \cdot u_{T_{\mathrm{fp\_02}} - T_{\mathrm{fp\_CMH}}}} \tag{3}$$

where the correlation coefficient ρ has been assumed equal to 1 and $u_{T\mathrm{fp\_03} - T\mathrm{fp\_CMH}}$ and $u_{T\mathrm{fp\_02} - T\mathrm{fp\_CMH}}$ are the standard uncertainties respectively of the difference between $T_{\mathrm{fp\_03}}$ and the frost-point temperature measured by the hygrometer $T_{\mathrm{fp\_CMH}}$ and between $T_{\mathrm{fp\_02}}$ and $T_{\mathrm{fp\_CMH}}$. The uncertainties represented in the plot correspond to the expanded combined uncertainty with a coverage factor k = 2. At -20 °C the difference between the INRIM 03 and the INRIM 02 frost-point temperature results to be $(T_{\mathrm{fp\_03}} - T_{\mathrm{fp\_02}})$ = (0.011 ± 0.148) °C, while at -75 °C is $(T_{\mathrm{fp\_03}} - T_{\mathrm{fp\_02}})$ = (0.160 ± 0.260) °C. The measurements provided by the two humidity generators are consistent within their expanded combined uncertainties, although at -75 °C the difference between the two generators is an order of magnitude greater than that one at -20 °C due to the poor reproducibility of CMH.

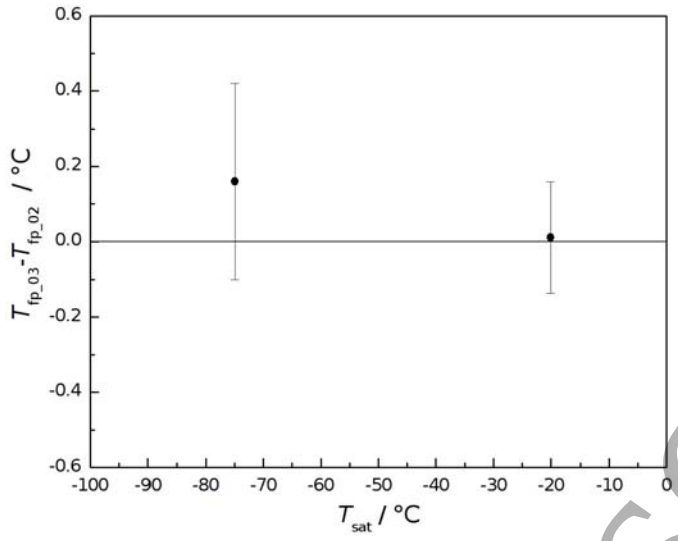

Figure 14. Difference values between the frost-point temperature generated by the INRIM 03 and the frost-point temperature generated by the INRIM 02 at two different saturated gas temperatures (-20 °C and -75 °C), P = 1100 hPa and ϕ = 1.5 l·min^{-1}.

6. Case study: comparison of performance of two CRDS analysers

INRiM 03 generator has been constructed with the aim to create a calibration facility for upper-air humidity sensors, such as radiosondes. However, at the moment it has been used exclusively to investigate and compare the performances of two different models of Tiger Optics trace gas moisture analysers: the HALO-RP M7005 and the SPARK model. Main properties of CRDS analysers taken from data sheets are reported in table 5.

Table 5. Main data sheet properties of HALO and SPARK CRDS.

Instrument properties	HALO	SPARK
Operating range	0 – 10 ppmv	0 - 2000 ppmv
Lowest detection limit	2 ppb	15 ppb peak-to-peak
Accuracy	4% of reading	4% of reading
Sample inlet pressure	80 – 2650 hPa	0.1 – 0.9 MPa

Both instruments, placed in parallel to each other, have been connected to the outlet of the generator. Thus, the humid gas generated by the INRIM 03 supplies in the same time both the analysers. For the investigation of the CRDS performances, a flow of humid nitrogen generated at a constant pressure of about 1100 hPa and at different values of frost-point temperature included between -90 °C and -65 °C has been used. In figures 15 the amounts of water vapour measured by the two analysers are shown as a

function of the frost-point temperature T_{fp} of the humid gas generated by the INRIM 03. The black line represents the theoretical water vapour amount generated by the INRiM 03, x_{w_0}, used as reference value, while squares and bullets represent the water vapour mole fraction measured respectively by the Halo and the Spark analyser, both indicated with the symbol x_{w_CRDS} for practical reasons.

Figure 15 highlights an overall agreement between values measured by the two CRDS within their expanded combined uncertainty, determined as square root of the sum of squares of their accuracy as given by the manufacturer and measurement repeatability, in addition to an overall agreement with the reference value, although the accuracy of the Spark analyser results to be lower than that of the Halo CRDS due to its construction features.

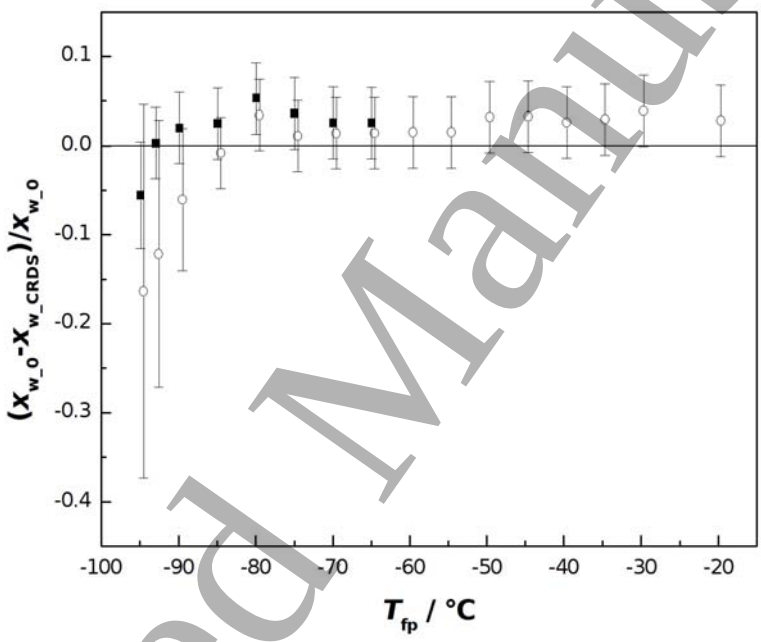

Figure 15. HALO analyser (■) and SPARK analyser (○) measurements of water vapour mole fraction, x_{w_CRDS}, as a function of the frost point temperature T_{fp} of the INRIM 03. The theoretical water vapour mole fraction generated by INRiM 03, x_{w_0}, is used as reference value. Uncertainties with a coverage factor $k = 2$.

7. Conclusions

To meet climatological community needs, a calibration facility for upper-air humidity sensors has been designed and constructed at INRIM. This facility can generate a humid gas with characteristics similar to those encountered in atmosphere during sounding operations in terms of pressure, temperature and water vapour amount fraction. It consists in a new low-frost point primary generator INRIM 03, which is able to operate at sub-atmospheric pressure (from 200 hPa to 1100 hPa) and in a wide range of frost point

temperature (-99 °C to -20 °C). This generator extends the INRIM humidity measurement capabilities downwards to -99 °C.

A preliminary uncertainty evaluation for the frost-point temperature down to -75 °C at atmospheric pressure and the corresponding water vapour mole fraction has been performed, resulting in an uncertainty $u_c(T_{fp}) = 0.015$ °C and $u_c(x_w) = 1.1 \cdot 10^{-8}$ respectively. A more detailed uncertainty evaluation on the generated x_w and T_{fp} in the whole working range is still underway. A comparison between the INRiM 03 and the well-established standard humidity generator INRIM 02 has been carried out showing an agreement within the expanded combined uncertainty. Finally, a comparison of performance of two CRDS analysers using the INRIM 03 has been shown as case study.

Acknowledgments

The present work has been carried out within the European Joint Research Project "MeteoMet 2 - Metrology for Essential Climate Variables" co-funded by the European Metrology Research Programme (EMRP). The EMRP is jointly funded by the EMRP participating countries within EURAMET and the European Union.

The authors would like to thank Tiger Optics that furnished the SPARK Cavity Ring Down Spectroscopy Analyser and gave the opportunity to test the instrument with the new low frost point generator (INRiM 03).

Moreover, the authors would like to thank their colleague Mauro Banfo for his everyday precious assistance and technical support and Francesca Botto for her rigor, attention and dedication to the scientific work.

References

[1] Craik D J and Miller B F 1958 The flow properties of powders under humid conditions *J. Pharm. Pharmacol.* 10 136T-144T

[2] Moreya R and Peleg M 1981 Effect of equilibrium water activity on the bulk properties of selected food powders *J. Food Sci.* **46** 1915-22

[3] Saunders S R J, Monteiro M and Rizzo F 2008 The oxidation behaviour of metals and alloys at high temperatures in atmospheres containing water vapour: a review *Prog. Mater. Sci.* **53** 5 775-837

[4] Tsutsumi H, Tanabe S, Harigaya J, Iguchi Y and Nakamura G 2007 Effect of humidity on human comfort and productivity after step changes from warm and humid environment *Build. Environ.* **42** 12 4034-42

[5] Körner O and Challa H 2003 Process-based humidity control regime for greenhouse crops *Comput Electron Agr* **39** 3 173-92

[6] Shindell D T 2001 Climate and ozone response to increased stratospheric water vapor *Geophys. Res. Lett.* **28** 8 1551-54

[7] Bojinski S, Verstraete M, Peterson T C, Richter C, Simmons A and Zemp M 2014 The concept of essential climate variables in support of climate research, applications, and policy *Bull. Amer. Meteor. Soc.* **95** 9 1431-43

[8] Feistel R *et al.* 2016 Metrological challenges for measurements of key climatological observables: oceanic salinity and pH, and atmospheric humidity. Part1: overview *Metrologia* **53** R1-R11

[9] Fernicola V, Bell S, Benyon R, Bose N, Georgin E, Heinonen M, Hudoklin D and Sargent M 2012 A European roadmap for humidity and moisture *EURAMET TC-T*

[10] Palchetti L, Bianchini G, Carli B, Cortesi U and Del Bianco S 2008 Measurement of the water vapour vertical profile and of the Earth's outgoing far infrared flux *Atmos. Chem. Phys.* **8** 2885-94

[11] Sherwood S C, Roca R, Weckwerth T M and Andronova N G 2010 Tropospheric water vapour, convection, and climate *Rev. Geophys.* **48** RG2001 1-29

[12] Dirksen R J, Sommer M, Immler F J, Hurst D F, Kivi R and Vomel H 2014 Reference quality upper-air measurements: GRUAN data processing for the Vaisala RS92 radiosonde *Atmos. Meas. Tech.* **7** 4463-90

[13] Wang J, Zhang L, Dai A, Immler F, Sommer M and Vomel H 2013 Radiation dry bias correction of Vaisala RS92 humidity data and its impacts on historical radiosonde data *J. Atmos. Oceanic Technol.* **30** 197-214

[14] Elliot W P and Gaffen D J 1991 On the utility of radiosonde humidity archives for climate studies *Bull. Amer. Meteor. Soc.* **72** 10 1507-20

[15] Vömel H GRUAN Lead Centre 2008-2014, Lindenberg, Germany 2012 private communication

[16] Miloshevich L M, Vömel H, Whiteman D N and Leblanc T 2009 Accuracy assessment and correction of Vaisala RS92 radiosonde water vapor measurements *J. Geophys. Res.* **114** D11305 1-23

[17] *GCOS reference upper-air network (GRUAN): Justification, requirements, siting and instrumentation options*, April 2007 GCOS-112 (WMO/TD No.1379)

[18] Scace G E and Hodges J T, Uncertainty of the NIST low frost-point humidity generator in *Proceedings of TEMPMEKO 2001, 8th International Symposium on temperature and thermal Measurements in Industry and Science, ed. By B. Fellmuth, J. Seidel, G.Scholz (VDE Verlag, Berlin, 2002)*, p. 597.

[19] Scace G E, Huang P H, Hodges J T, Olson D A and Whetstone J R The new NIST low frost-point humidity generator in *Proceedings of the NCSL 1997 Workshop and Symposium* (Atlanta, 1997), p. 657.

[20] Scace G E, Hovde D C, Hodges J T, Huang P H, Silver J A and Whetstone J R, Performance of a precision low frost-point humidity generator in *Proceedings of 3rd International Symposium on Humidity and Moisture*, vol 1 (NPL, 1998).

[21] Mamontov G 2000 Application of the phase equilibrium method for generation of −100 ℃ of humid gas frost-point temperature *Meas. Sci. Technol.* **11** 818–27

[22] Choi B I, Nham H S, Woo S B, Kim J C and Kwon S Y, 2008 The new KRISS low frost-point humidity generator *Int. J. Thermophys.* **29** 1578-1588

[23] Choi B I, Kim J C and Woo S B 2012 Uncertainty of the KRISS low frost-point humidity generator *Int. J. Thermophys.* **33** 1559-1567

[24] Choi B I, Lee S –W, Kim J C, Woo S B 2015 Extension of humidity standards to -105 °C frost point *Int. J. Thermophys.* **36** 2231-2241

[25] Venzke H, Schirmer B, Still M, Melling A and Durst Franz 2000 Fast trace humidity generation in the 0.1 ppm to 1000 ppm range with a two-stage dilution and mixing generator *Meas. Sci. Technol.* **11** 1732-1743

[26] Lovell-Smith J 2009 The propagation of uncertainty for humidity calculations *Metrologia* **46** 607–15

[27] Sonntag D 1990 Important new values of the physical constants of 1986, vapour pressure formulations based on the ITS-90, and psychrometer formulae *Z. Meteorol.* **40** 340–4

[28] Greenspan L 1976 Functional equations for the enhancement factors for CO2-free moist air *J. Res. Natl. Bur. Stand.* **80A** 41–4

[29] Lovell-Smith J 2007 An expression for the uncertainty in the water vapour pressure enhancement factor for moist air *Metrologia* **44** L49-52

[30] Tulegenov A S, Wheatley R J, Hodges M P and Harvey A H 2007 Intermolecular potential and second virial coefficient of the water-nitrogen complex *J. Chem. Phys.* **126** 094305

[31] Johnson D P 1974 Note on diffusion of vapour into flowing gas *J. Res. Nat. Bur. Stand.* **78A** 49-51

[32] Fernicola V and Arpino F 2010 Design and modelling of a low frost-point humidity generator *Proc. Joint Int. Symp. on Temperature, Humidity, Moisture and Thermal Measurements in Industry and Science (Portoroz, Slovenia)*

[33] Meyer C W, Hodges J T, Huang P H, Miller W W, Ripple D C and Scace G E 2008 Calibration of hygrometers with the hybrid humidity generator *Natl. Inst. Stand. Technol. Spec. Publ.* **250-83**

[34] kcdb.bipm.org/appendixC/T/IT/T_IT.pdf

[35] Actis A, Fernicola V and Banfo M, 1999 Characterization of the IMGC frost point generator in the temperature range -75 °C to 0 °C *Proc. 7th Int. Symp. on Temperature and Thermal Measurement in Industry and Science (Delft, Netherlands)*

[36] Bell S *et al.* 2015 Final report to the CCT on key comparison CCT-K6 – Comparison of local realisations of dew-point temperature scales in the range -50 °C to +20 °C *NPL report ENG 57* **ISSN 1754-2987**

[37] Heinonen M 2010 Report to the CCT on key comparison EUROMET.T-K6 (EUROMET Project no. 621): Comparison of the realizations of local dew/frost-point temperature scales in the range −50 °C to +20 °C *Metrologia* **47** 03003